Available online at www.sciencedirect.com
SCIENCE DIRECT®
Combustion and Flame 143 (2005) 183–198
Combustion and Flame
www.elsevier.com/locate/combustflame

Modeling of marginal burning state of fire spread in live chaparral shrub fuel bed ☆

Xiangyang Zhou [a,*], Shankar Mahalingam [a], David Weise [b]

[a] *Department of Mechanical Engineering, University of California, Riverside, CA 92521, USA*
[b] *Forest Fire Laboratory, Pacific Southwest Research Station, USDA Forest Service, 4955 Canyon Crest Drive, Riverside, CA 92507, USA*

Received 21 October 2004; received in revised form 1 May 2005; accepted 11 May 2005

Available online 20 July 2005

Abstract

Prescribed burning in chaparral, currently used to manage wildland fuels and reduce wildfire hazard, is often conducted under marginal burning conditions. The relative importance of the fuel and environmental variables that determine fire spread success in chaparral fuels is not quantitatively understood. Based on extensive experimental study, a two-dimensional numerical model for vegetation fire spread was developed to simulate laboratory-scale fires. This model is based on a detailed description of the complex heat transfer processes and a simple combustion mechanism contributing to the ignition of solid fuel and fire spread. The fuel bed is described as a porous medium, and the heterogeneous nature of foliage and branch is considered via specific physical properties such as surface area-to-volume ratio, density, and volume fraction. The burning of solid fuel is computed by solving mass and energy equations, including the effects of drying, pyrolysis, and char combustion and the exchanges of mass, momentum, and energy with the surrounding gas. The effects of wind, slope, fuel moisture content, fuel bed arrangement, environmental temperature, and humidity are considered in the numerical model. Computations were performed to compare successful and unsuccessful fire spread cases to highlight the effects of various factors. Numerical results were consistent with the experimental observations of the transition between no fire spread and spread under different fuel and environmental conditions. The simulated heat transfer processes and combustion mechanism in the fuel bed are helpful in identifying factors that determine fire spread success. It was found that the relative importance of modeled convective and radiative heat transfer processes to ignition of solid fuel differed with particle location, and could be switched depending on the wind speed, terrain slope, and fuel bed arrangement.
© 2005 The Combustion Institute. Published by Elsevier Inc. All rights reserved.

Keywords: Marginal burning; Chaparral; Modeling; Fire spread

1. Introduction

Wildland fire has been a part of the Southern California landscape for centuries. The mountains of Southern California and throughout the coastal ranges are covered at lower elevations (below 1600 m) with chaparral vegetation characteristic of Mediterranean climates (see Fig. 1). Chaparral is a highly

☆ The U.S. Government's right to retain a nonexclusive royalty-free license in and to the copyright covering this paper, for governmental purposes, is acknowledged.

* Corresponding author. Fax: +1 951 827 2899.
E-mail address: xzhou@engr.ucr.edu (X. Zhou).

0010-2180/$ – see front matter © 2005 The Combustion Institute. Published by Elsevier Inc. All rights reserved.
doi:10.1016/j.combustflame.2005.05.013

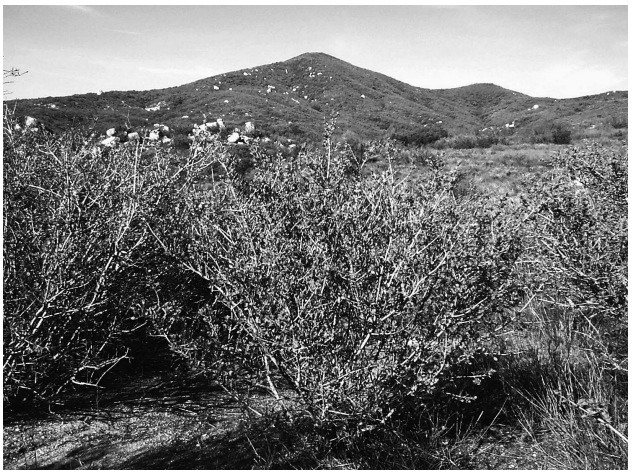

Fig. 1. A highly flammable shrub complex, chaparral, grows in the foothills of California. Note that the fuel is located at some distance from the ground and the topography of the terrain is highly variable.

flammable shrub complex that includes different species such as manzanita (*Arctostaphylos glandulosa*), chamise (*Adenostoma fasciculatum*), hoaryleaf ceanothus (*Ceanothus crassifolius*), and scrub oak (*Quercus berberidifolia*) [1]. Fuel depths observed in chaparral crowns range from 30 to 300 cm and vary by species, elevation, slope, and rainfall. The height of chaparral stands ranges from 1 to 6 m, and the crowns tend to be fairly porous.

Prescribed burning is often used as a tool to manage wildland fuels and reduce wildfire hazard [2]. Land management agencies in California actively use prescribed fire to burn fire-prone brush land to prevent wildfires. Prescribed burning in chaparral is typically attempted in the spring to early summer or following winter rains when fuel moistures are higher in most cases than when wildfires occur [3]. Because of the risk of escaped fire, prescribed burning is often conducted under marginal burning conditions in which the fire either spreads or fails to spread after ignition. Marginal burning conditions result in low-intensity fires that can be controlled relatively easily and often produce a mosaic of burned and unburned vegetation that is a desirable habitat for many animals. Under these conditions, there seems to be a threshold between no fire spread and successful propagation. Researchers have reported thresholds in fire behavior as influenced by various fuel and environmental variables [4]. Wilson [5] developed a "predictive rule of thumb" to determine if fires would burn in wooden fuel beds. The matrix approach [6] links a quasi-quantitative description of fire behavior and effects to a score computed from severity points assigned to various values of fuel and weather variables. Both the matrix approach and the Campbell Prediction System [7] use basic understanding of the variables that influence fire behavior to arrive at predictions. McCaw [8] summarized many of these studies.

In California, at least two operational versions of the Rothermel spread model [9] are employed by fire managers to aid in the use of prescribed fire [10,11]. The Rothermel model is a semi-empirical model that was derived by parameterizing a solution of the conservation of energy equation [12]. The constants necessary to close the system were evaluated from experimental fires under simplified conditions with dead fuel material. The Rothermel and other semi-empirical models [13] provide a good approximation of the fire spread rate under conditions that are close to experimental conditions under which model parameters were obtained and calibrated. However, the use of these models for more general prescribed fire conditions does not always give satisfactory results because they were not designed primarily for live fuels and marginal burning conditions. One example is that fire spreads successfully in chaparral fuels at fuel moistures higher ($>60\%$) than those in most of the experimental data used to develop the Rothermel model ($<30\%$) for no wind and flat ground conditions. The main reason is that these models do not completely describe the physical mechanisms that control thermal degradation of solid fuel, the fire behavior, and the solid–flame interactions [14]. The various heat transfer mechanisms of radiation, convection, and conduction are not explicitly described.

To improve the capability of numerical prediction of marginal burning during prescribed burning in live chaparral, a more complete approach based on physical considerations needs to be adopted. In contrast to most statistical and empirical models for large-scale propagating wildfires, the present model and other models [14–20] belong to the class of small-scale

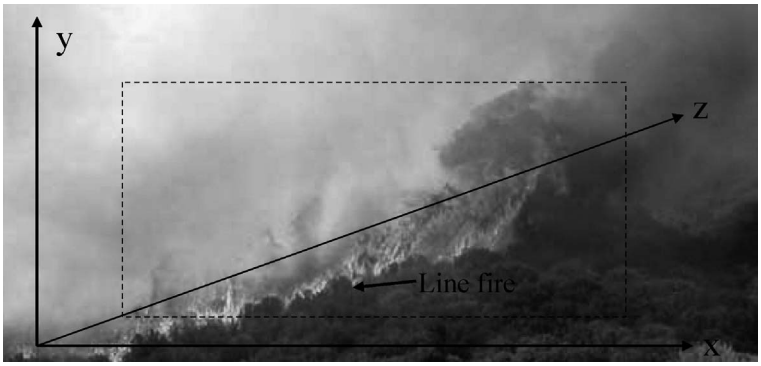

Fig. 2. Wildland fire spread through the shrub fuel bed and the fire front is assumed to have a rectilinear shape (line fire).

physical models. In such models, the multiple interactions between the gaseous phase and the solid fuel are described in detail to obtain a complete representation of the physical mechanisms (gas flow, combustion, radiation, and convective heat transfer) contributing to the thermal decomposition (vaporization, pyrolysis, char oxidation) occurring during the development of a wildland fire. Adopting an averaging formulation to the conservation equations (mass, momentum, energy, species concentration), the coupling between the solid and the gaseous phases is modeled through source terms in the mass (decomposition of solid fuel to combustible gas), momentum (drag force), and energy (heat transfer by convection and radiation) balance equations. The fuel bed is approximated as a uniformly distributed porous medium (solid particles), characterized by geometrical (surface-to-volume ratio, packing ratio, fuel depth), physical, and chemical (fuel density, reaction rates and composition of the pyrolysis products, moisture content) properties evaluated experimentally. Environmental factors including wind speed and direction, terrain slope, temperature, and relative humidity are also considered. Given the increased complexity of this model, it is applied to simulate laboratory-scale experiments and small or medium-scale surface in which a two-dimensional approximation may be assumed [14]. In a large-scale wildland fire, the fire front is generally represented as a curve separating burnt area from fresh fuel. In a small region or in a controlled laboratory-scale fire, the fire front can be assumed to have a rectilinear shape (line fire), and the direction of fire spread through the fuel bed can be assumed to be perpendicular to the fire front. Therefore, a 2D simplification (a vertical plane defined by the direction of propagation x and the vertical direction y, see Fig. 2) is often used to analyze fire propagation [13–22]. Although the flames exhibit fully three-dimensional behavior, over a small portion of the fire front, the major contributions concerning the heat balance inside the fuel bed and above the shrub fuel can be approximated as two-dimensional.

Given that current operational models do not adequately model fire spread in chaparral fuels and that data describing marginal burning conditions in chaparral do not currently exist, we embarked on an experimental effort to determine the important fuel and environmental variables that determine propagation success in laboratory-scale fires in common chaparral fuels. From these data, a statistical model to predict the probability of successful fire spread was developed using stepwise logistic regression [23,24].

Because of the limitations in the experimental diagnostics available to us, the detailed flame structure and the heat transfer processes are not accessible. The aim of the present work is to describe the physical nature of marginal burning and the propagation of experimental fires in live chaparral shrub fuels. Using a numerical model based on detailed physical considerations, we have simulated fire experiments for varying values of fuel bed depth, fuel loading, fuel moisture content, wind speed, slope, and environmental temperature. By analysis of the velocity, temperature, species concentration fields, and heat transfer processes through radiation and convection that occur in the fuel bed, it is possible to gain a better understanding of the fuel and environmental variables that determine fire spread success.

For the current purpose of studying marginal burning, whether or not fire can spread under various conditions, we focus on the main physical mechanisms to determine the ignition of chaparral fuel. Thus, the 2D approximation used for the present study is a compromise designed to reduce computational time, yet allow for a detailed study of the major contributing factors governing fuel ignition and fire spread. This compromise is reasonable when the vegetation is uniformly distributed over the transverse z direction (the direction ignored by the 2D approximation, Fig. 2) and when we consider the head of a fire, where the

directions of the wind, the slope, and the direction of the fire propagation are parallel.

2. Mathematical formulation and modeling

2.1. Solid phase

In the present approach, the shrub fuel bed is considered a porous medium. It is a heterogeneous system made of a solid matrix with randomly oriented structure. In a small control volume V, the solid phase coexists with the gas phase. The porosity is defined as $\xi = V_g/V$, where V_g is the volume occupied by gas, and the packing ratio is defined as $\beta = V_s/V$, with the condition $\xi + \beta = 1$. For fire spread, the key process is the transfer of mass, momentum, and energy between the gas and solid phases. These transfers are directly related to the specific wetted area $A = \beta\sigma_s$, where σ_s is the ratio of surface area to volume of the solid phase.

For cylindrical fuels, σ_s can be approximated from the equation $\sigma_s = 4/d$, where d denotes diameter of fuel particles. Under their experimental conditions, Fons et al. [25] found that ignition time decreased with increasing σ_s, and the rate of fire spread increased linearly with increase in σ_s. The difference in σ_s for foliage and branches of different size is pronounced. For example, for a 3.2-mm-diameter branch, $\sigma_s = 1250\ \mathrm{m}^{-1}$, whereas for a 25.4-mm-diameter branch, $\sigma_s = 157\ \mathrm{m}^{-1}$. For foliage, σ_s ranges from 4000 to 7000 m^{-1}. Considering the range of σ_s and its influence on fuel combustion, it is reasonable to model the solid fuel as consisting of two phases: foliage (higher value of σ_s) and branches (lower value of σ_s). These two phases have different density but are assumed to have the same moisture content.

To simplify the problem, it is assumed that the shrub fuel initially includes water, pyrolyzates, char, and noncombustible ash (or minerals). Some high-energy ether extractives (waxes, oils, terpenes, and fats) present in live chaparral shrub fuels are not considered because very little information is available on their role in fire spread [26,27]. Taking into account water vaporization, pyrolysis, and char combustion within the preheating and burning processes, the mass balance equation for the solid phase is expressed as

$$\frac{\partial m_s}{\partial t} = -\omega_{s,H_2O} - \omega_{s,pyr} - \omega_{char}, \tag{1}$$

where t is time, m_s is the mass of the solid phase including water (m_{s,H_2O}), pyrolysis ($m_{s,pyr}$), char ($m_{s,char}$), and ash. The rates of solid mass reduction due to drying, pyrolysis, and char oxidation, denoted by ω_s with appropriate subscripts, are deduced from Arrhenius-type laws. The mass of ash included in the solid phase is assumed to be constant. Because no data are currently available for chaparral fuels, the kinetic parameters for the rates (expressed in $\mathrm{kg/m^3/s}$) are taken from the model of Porterie et al. [16] for pine needles as

$$\omega_{s,H_2O} = 6.0 \times 10^5 T_s^{-0.5} m_{s,H_2O} \times \exp(-5800/T_s), \tag{2}$$

$$\omega_{s,pyr} = 3.63 \times 10^4 m_{s,pyr} \exp(-7250/T_s), \tag{3}$$

$$\omega_{char} = \frac{1}{r_2} 430.0 A_s \rho_{O_2} \exp(-9000/T_s), \tag{4}$$

where r_2 is the oxygen-to-carbon stoichiometric mass ratio, T_s is the solid fuel temperature, and ρ_{O_2} is the density of oxygen. Here, char is idealized as pure carbon and the heterogeneous reaction is assumed to be: $C + O_2 \Rightarrow CO_2$ ($r_2 = 8/3$).

A successful fire spread depends on the condition that sufficient heat can be transferred from the flame front to the unburnt solid fuel, thereby raising its temperature to the ignition point. The variation in solid-phase temperature is the result of radiative and convective transfer rates $Q_{rad,s}$ and Q_{conv} between the solid and the gas. The heat loss/absorption rate Q_{mass}, due to water vaporization, pyrolysis, and char oxidation, also influences the solid-phase temperature. Invoking the assumption that fuel particles are thermally thin, the energy balance equation for the solid phase reduces to

$$m_s c_{ps} \frac{\partial T_s}{\partial t} = Q_{conv} + Q_{rad,s} + Q_{mass}. \tag{5}$$

In Eq. (5), the specific heat of the solid phase, c_{ps}, is deduced from that of dry wood material and the fractional mass moisture, $Y_s^{H_2O}$, remaining in the fuel material:

$$c_{ps} = \left(1 - Y_s^{H_2O}\right) c_p^{dry} + Y_s^{H_2O} c_p^{H_2O}. \tag{6}$$

The convective heat transfer rate between the gas and solid phases is calculated as

$$Q_{conv} = A h_c (T - T_s), \tag{7}$$

where the heat transfer coefficient h_c is deduced from the Nusselt number Nu of the solid phase [28],

$$\mathrm{Nu} = \frac{h_c d}{\lambda} = 0.683\,\mathrm{Re}^{0.466}, \tag{8}$$

where λ is the conductive heat transfer coefficient of the gas phase, and the Reynolds number Re is based on the surface area per unit volume ratio for a cylindrical shape $d = 4/\sigma_s$. The rate of heat release due to water vaporization and pyrolysis and heat absorption due to fuel combustion, Q_{mass}, is

$$Q_{mass} = -\omega_{s,H_2O} L^{H_2O} - \omega_{s,pyr} L^{pyr} + X_c \omega_{char} L^{char}. \tag{9}$$

Water vaporization is an endothermic process ($L^{H_2O} = 2250$ kJ/kg) while char combustion is highly exothermic ($L^{char} = 32740$ kJ/kg). Pyrolysis is assumed to be slightly endothermic ($L^{pyr} = 0.418$ kJ/kg). The variable X_c is a sharing coefficient describing the distribution of the heat of char combustion between solid and gas phases. For the present case it is assumed $X_c = 0.5$. Finally, in Eq. (5), the radiative heat transfer rate through the solid matrix $Q_{rad,s}$, is an important heat transfer mechanism during the propagation of a wildfire. This is described in the next subsection.

2.2. Gas phase

Airflow, combustion of pyrolysis fuel gas, and heat transfer through the gas phase are all important processes in a successful fire spread. Based on the porous medium assumption for solid fuel, for two-dimensional unsteady flow, the Favre- or density-weighted averaged conservation equation of the gas phase for mass is described as

$$\frac{\partial \bar{\rho}}{\partial t} + \frac{\partial}{\partial x}(\bar{\rho}\tilde{u}) + \frac{\partial}{\partial y}(\bar{\rho}\tilde{v}) = S_{\text{s-g}}, \tag{10}$$

where $\bar{\rho}$ is the mean gas density, and x and y denote horizontal and vertical spatial coordinates with $\tilde{u}$ and $\tilde{v}$ denoting Favre-averaged velocity components along these directions. The source term $S_{\text{s-g}}$ is the average production rate term resulting from the decomposition of solid fuel (drying, pyrolysis, char oxidation) to gas phase. Because solid coexists with gas in the fuel bed, the control volume for gas-phase calculation is reduced to ξV.

The governing equations for momentum in Cartesian tensor notation are

$$\frac{\partial \bar{\rho}\tilde{u}_i}{\partial t} + \frac{\partial}{\partial x_j}(\bar{\rho}\tilde{u}_j\tilde{u}_i) = -\frac{\partial \bar{p}}{\partial x_i} + \frac{\partial}{\partial x_j}\left[\mu_{\text{eff}}\left(\frac{\partial \tilde{u}_i}{\partial x_j} + \frac{\partial \tilde{u}_j}{\partial x_i}\right)\right] + \bar{\rho} g_i - \bar{F}_{s,i}, \tag{11}$$

where the effective eddy viscosity $\mu_{\text{eff}} = \mu + \mu_t$ is evaluated from the turbulent kinetic energy k and its dissipation rate ε, using the classic relation $\mu_t = C_\mu \bar{\rho} k^2/\varepsilon$ with $C_\mu = 0.09$ [29]. The variable g_i denotes the gravitational acceleration vector and $\bar{p}$ the pressure. The quantity $F_{s,i}$ represents the ith component of the drag force resulting from the interaction between the gas and solid phases. It is approximated as $F_{s,i} = 0.5 C_D \bar{\rho} A |u| \tilde{u}_i$. The drag coefficient C_D depends on the Reynolds number [30], and is approximated as $C_D = 24(1 + 0.15\,\text{Re}^{0.687})/\text{Re}$.

To take into account the contribution of the turbulent fluctuations, a two-equation k-ε turbulence model is adopted. The governing equations are given by

$$\frac{\partial \bar{\rho} k}{\partial t} + \frac{\partial}{\partial x_j}(\bar{\rho}\tilde{u}_j k) = \frac{\partial}{\partial x_j}\left[\left(\mu + \frac{\mu_t}{\sigma_k}\right)\frac{\partial k}{\partial x_j}\right] + P_k - \bar{\rho}\varepsilon + D_1, \tag{12}$$

$$\frac{\partial \bar{\rho} \varepsilon}{\partial t} + \frac{\partial}{\partial x_j}(\bar{\rho}\tilde{u}_j \varepsilon) = \frac{\partial}{\partial x_j}\left[\left(\mu + \frac{\mu_t}{\sigma_\varepsilon}\right)\frac{\partial \varepsilon}{\partial x_j}\right] + \frac{\varepsilon}{k}(C_1 P_k - C_2 \bar{\rho}\varepsilon) + D_2, \tag{13}$$

where P_k denotes the generation rate of turbulent kinetic energy and, in the present case due to buoyancy and shear effects, is given by

$$P_k = \mu_t\left(\frac{\partial \tilde{u}_i}{\partial x_j} + \frac{\partial \tilde{u}_j}{\partial x_i}\right)\frac{\partial \tilde{u}_i}{\partial x_j} + \frac{1}{\rho}\frac{\mu_t}{\text{Pr}}\frac{\partial \bar{\rho}}{\partial x_i} g_i. \tag{14}$$

Because of the presence of solid shrub fuel, two source terms D_1 and D_2 are introduced to take into account the turbulent kinetic energy and its dissipation rate in the wake of solid fuel [31,32]. Although there are different scales involved in the shear-generated and wake eddies, in the present work, only total turbulent kinetic energy is considered to minimize modifications to the k-ε model. The two source terms are thus modeled by

$$D_1 = \frac{1}{2}\bar{\rho} A C_D |u||u|^2, \tag{15}$$

$$D_2 = \frac{1}{2}\frac{\varepsilon}{k} C_3 \bar{\rho} A C_D |u||u|^2. \tag{16}$$

The empirical constants are $\sigma_k = 1.0$, $\sigma_\varepsilon = 1.3$, $C_1 = 1.44$, $C_2 = 1.92$, $C_3 = 1.95$, and $\text{Pr} = 0.7$ [31].

For wildland fuels, the composition of the pyrolysis products is complicated (C, CO, CO_2, H_2O, CH_4, H_2, C_2H_6, ...) and temperature dependent. To simplify the problem, the most representative components of pyrolysis gas are taken to be CO and CO_2, and only five chemical gas species (CO, CO_2, H_2O, O_2, and N_2) are considered to describe fuel gas, air, and products of combustion. The general governing equation of mass fraction (Y_i) of gas species is

$$\frac{\partial \bar{\rho}\tilde{Y}_i}{\partial t} + \frac{\partial}{\partial x_j}(\bar{\rho}\tilde{u}_j \tilde{Y}_i) = \frac{\partial}{\partial x_j}\left(\Gamma_{\text{eff},Y_i}\frac{\partial \tilde{Y}_i}{\partial x_j}\right) + S_{\text{s-g},i} + \omega_i. \tag{17}$$

The turbulent fluxes of gas species are approximated using an effective exchange coefficient, $\Gamma_{\text{eff}} = \mu_{\text{eff}}/\text{Pr}$. The source term $S_{\text{s-g},i}$ is the average production rate of gas species i resulting from the decomposition of solid fuel accompanied by vaporization, pyrolysis, and char oxidation. The source term ω_i is the production/destruction rate of chemical species as a result of homogeneous combustion in the gas phase.

The combustion model is based on the eddy-dissipation model of Magnussen and Hjertager [33]. In diffusion flames, fuel and oxygen are presumed to be present in separate eddies. Because the chemical

reactions in most cases are very fast, it can be assumed that the rate of combustion will be determined by the rate of intermixing on a molecular scale of fuel and oxygen eddies, in other words, by the rate of dissipation of the eddies. Consequently, the fuel reaction rate ω_i, is taken to be the slowest of the turbulence dissipation rates corresponding to fuel and oxygen,

$$\omega_i = -C_R \bar{\rho} \frac{\varepsilon}{k} \min\left[\tilde{Y}_{fu}, \frac{\tilde{Y}_{ox}}{r}\right], \tag{18}$$

where r is the stoichiometric ratio of the chemical reaction $CO + 0.5O_2 \Rightarrow CO_2$ ($r = 4/7$), and C_R is a dimensionless coefficient suggested by Magnussen et al. [34] in functional form via $C_R = 23.6(\nu\varepsilon/k^2)^{0.25}$, where ν is the kinematic viscosity.

The thermal energy equation of the gas phase is described through temperature via

$$\frac{\partial \bar{\rho} c_p \tilde{T}}{\partial t} + \frac{\partial}{\partial x_j}(\bar{\rho}\tilde{u}_j c_p \tilde{T}) = \frac{\partial}{\partial x_j}\left(c_p \Gamma_{eff,T} \frac{\partial \tilde{T}}{\partial x_j}\right) - Q_{conv} + Q_{rad} + Q_{reac} + (1 - X_c)\omega_{char} L^{char}, \tag{19}$$

where $\Gamma_{eff,T} = \mu_{eff}/\mathrm{Pr}$ is the effective exchange coefficient of energy describing turbulent fluctuations. Among the source terms, Q_{conv} denotes the convective/conductive heat transfer between gas and solid phases, Q_{rad} the radiative heat transfer, and Q_{reac} the heat released from the combustion of pyrolysis fuel gas. The last term on the right-hand side of Eq. (19) describes a part of heat released from heterogeneous combustion between char and oxygen.

2.3. Radiative heat transfer

As pointed out by many wildfire researchers [21, 22,35–37], the radiative heat transfer rate $Q_{rad,s}$ through the solid matrix is one of the important heat transfer mechanisms during the propagation of a wildfire. Radiation arises mainly from soot particles produced in the flame and from the burning of solid fuels. Including these two contributions, an extension of the discrete ordinates (DO) method [38] to porous media was developed to calculate radiation through the solid matrix and radiative heat transfer between gas and solid phases. This DO method is well adapted to solve the problem of radiative transfer in a medium presenting significant variations of the absorptions. For a specific ordinate direction i, defined by $\mathbf{\Omega}_i = (\mu_i, \eta_i)$, the two-phase radiative heat transfer equation can be written as

$$\mu_i \frac{\partial \xi I_i}{\partial x} + \eta_i \frac{\partial \xi I_i}{\partial y} = -\left(\xi a_g + \frac{\beta\sigma_s}{4}\right) I_i + \xi a_g \frac{\sigma T^4}{\pi} + \frac{\beta\sigma_s}{4}\frac{\sigma T_s^4}{\pi}, \tag{20}$$

where I_i is the radiative intensity in the direction $\mathbf{\Omega}_i$ with μ_i and η_i denoting the directional cosines with respect to the Cartesian coordinate system, and σ is the Stefan–Boltzmann constant. This equation is integrated over a control volume. The radiative heat source, which appears in the energy equation of the gas phase, is given by

$$Q_{rad} = \xi a_g (G - 4\sigma T^4). \tag{21}$$

In a similar way, the radiative heat source in the energy equation of the solid phase is

$$Q_{rad,s} = \frac{\beta\sigma_s}{4}(G - 4\sigma T_s^4). \tag{22}$$

In Eqs. (21) and (22), the average incident radiation can be approximated by $G = \sum_{i=1}^{N} w_i I_i$, where w_i are the appropriate weights of the quadrature. The medium properties are given by the absorption coefficients a_g and a_s for the gas and the solid phases, respectively. For propagation of a surface fire through pine needles or excelsior fuel beds, experimental measurements of the heat fluxes received by a radiometer had shown that the approximation used for the absorption coefficient, $a_s = \beta\sigma_s/4$, was verified with an error of less than 10% [39]. Following Kaplan et al. [40], the absorption of the soot/combustion product (CO_2, H_2O) mixture is evaluated by making the gray gas assumption from the mole fraction of the combustion products and the average soot volume fraction f_v:

$$a_g = 0.1(X_{CO_2} + X_{H_2O}) + 1862 f_v T \ (\mathrm{m}^{-1}). \tag{23}$$

Soot formation is described through the evolution of the average soot volume fraction f_v accounting for nucleation, surface growth, and oxidation processes

$$\frac{\partial}{\partial t}(\bar{\rho} f_v) + \frac{\partial}{\partial x_j}\left[\bar{\rho}\left(\tilde{u}_j + u_j^{th}\right) f_v\right] = \frac{\partial}{\partial x_j}\left(\frac{\mu_t}{\mathrm{Pr}}\frac{\partial f_v}{\partial x_j}\right) + \omega_{fv}, \tag{24}$$

where u_j^{th} is the mean thermophoretic velocity components given by Kaplan et al. [40]:

$$u_j^{th} = -0.54 \frac{\mu}{\bar{\rho}} \frac{\partial \ln T}{\partial x_j}. \tag{25}$$

Most of the soot is assumed to be formed as a result of devolatilization of vegetation fuels, and the source term in Eq. (24) takes the form

$$\omega_{fv} = \frac{\bar{\rho}}{\rho_{soot}}\left(0.01\omega_v - \frac{6 f_v}{d_{soot}} W_{NSC}\right). \tag{26}$$

The last term corresponds to the Nagle and Strickland–Constable (NSC) rate for oxidation by O_2 given in detail in Kaplan et al. [40]. The soot particle diameter d_{soot} is assumed to be 10 μm.

Fig. 3. Experimental setup of the fuel bed constructed of live foliage and branches of chamise with 2.0 m long, 1.0 m wide, and 0.2 m deep. The fire illustrates the initial ignition, and the ruler at the right side shows the scale with 0.25 m.

3. Experimental setup

The shrub fuel was collected from living chaparral that grows at an elevation of 1160 m in the North Mountain experimental area, 50 km east of Riverside, California (Fig. 3). Foliage and branches (diameter < 0.64 cm) from four chaparral species constituted the fuel. Fuel was harvested in the morning so as to minimize moisture loss through transpiration. Dead fuel was removed to the extent possible. The fuels were then bagged and transported to the burn facility at the Forest Fire Laboratory.

Fuel beds (2.0 m long, 1.0 m wide, and various depths: 0.4 and 0.2 m) were elevated above the surface of a tilting platform by 0.4 m to simulate an aerial fuel (Fig. 3). Air can be entrained from the bottom of the fuel bed. Fire spread in chaparral has been described as a crown fire by some researchers. Some laboratory-scale works have been done to estimate the effect of fire line width on the rate of spread of a fire. Fons et al. [25] and Anderson [41] suggested that a width of 30 cm or more would be enough to produce consistent rates of spread in a no-wind fire. From a series of field fire experiments, Wotton et al. [42] observed that the dependence of rate of spread on width becomes very weak for width > 2 m in a weak wind fire. Following the above analysis and the experimental setup of Catchpole et al. [43], the current fuel bed and experiment were designed. To mimic a wider fire front and to maintain a line fire spread case, air entrainment from the lateral sides of the fuel bed along the fire spread direction was prevented by metal sheeting. A fraction of the radiative heat flux was also reflected.

Fires were ignited from one side in a 50-cm section along the length of the live fuel bed. The ignition zone was set to provide sufficient ignition energy to initiate and sustain fire spread. Based on our experimental observation of a successful fire spread, it was found that fire spread reached a quasi-steady state after approximately half of the total length, and the observed flame length maintained roughly a constant value. After a line fire ignition, we observed that most of experimental fires maintain a rectilinear shape. The cases studied were limited to a 2D configuration. Fuel was uniformly distributed to the greatest extent possible. The effect of slope was induced by raising one end of the tilting platform. Airflow to simulate wind was induced using three rotary box fans, which were turned on simultaneously. Only two conditions, “wind” and “no wind,” were considered. The natural changes in live fuel moisture content, environmental temperature, and relative humidity were considered by collecting fuels and conducting experiments over the course of an annual cycle. For the purpose of characterizing marginal burning, an experiment was described as successful if the live brush fuel ignited from the burning zone and then propagated the length of the 2-m fuel bed. The experiment was considered unsuccessful if the fire did not propagate.

4. Numerical methods

The generic governing equations of momentum, energy, and species mass fractions are discretized using an implicit method in a 2D Cartesian coordinate system. Diffusion terms were approximated using a central difference scheme; convective terms

were discretized using a hybrid scheme. The pressure and velocity coupling is treated using the SIMPLER method [44]. The resulting systems of linear equations for each variable are then solved iteratively using the TDMA (tridiagonal matrix) algorithm. To ensure convergence and prevent low-frequency behavior of the solution typical of this type of buoyancy-driven flow, all the variables are underrelaxed using inertial relaxation. At each time step, an iterative procedure is used to calculate the new values at the next time step.

When the wind effect was considered, the wind velocity profile was prescribed as a boundary condition at the left edge of the computational domain. A power law boundary layer $\tilde{u}(y) = U_{\mathrm{ref}}(y/\delta_0)^{1/7}$ is used, and wind speed U_{ref} is given at height $\delta_0 = 0.7$ m. The slope effect was considered by rotating the Cartesian coordinate an angle θ that is the angle between the ground surface and a horizontal line. The x axis remains parallel to the ground. The gravitational acceleration vectors along x and y axes are $g_i \sin\theta$, and $g_i \cos\theta$, respectively. In topographic terminology, the slope percent is $100 \tan\theta$. For $\theta = 45°$, slope percent is 100%.

Open boundary conditions might exist at the inlet (upwind), top or lateral boundaries, and the outlet (downwind). At the outlet boundary, outflow or inflow conditions might exist during the temporal evaluation. Outflow conditions were taken to be zero derivatives for all the variables. If inflow occurs at the outlet boundary, temperature, oxygen mass fraction, etc., are taken as constant values because they are transported from the surrounding stagnation conditions. In short, upwind philosophy was considered at the outlet.

To model the experimental setup, a 2D computational domain 4.0 m long × 3.5 m high was designed. After the effect of grid resolution was examined, a nonuniform grid of 129 × 65 cells was used to cover the computational domain. The computational time step is 0.2 s. The fuel bed setup is identical to the laboratory experiment. However, to save computation time, the modeled fuel bed was 1.275 m long and thus shorter than the experimental fuel bed length. This is acceptable because the focus of this study is marginal burning concerning the initial ignition and subsequent propagation. The fuel bed depth is the same as in the experiment, viz., 0.4 m (or 0.2 m). A uniform grid of 51 × 16 cells was used to cover the fuel bed. The fuel bed is placed in the center of the computational domain along the horizontal direction. There is a gap of 0.4 m height with 10 nonuniform cells between the bottom of the fuel bed and the ground level. Air can be entrained into the bottom of the fuel bed. This setup modeled an aerial fuel. This arrangement was chosen to replicate chaparral brush fire in which fuel is located at some distance from the ground (see Fig. 1), as is the case with crown fires.

The properties of the chaparral fuels are obtained mainly from the experimental measurements of Countryman and Philpot [45]. The average fuel density of chaparral shrub is $\rho_s = 560$ kg/m^3, defined as the dry wood mass per unit green volume. The mean surface-to-volume ratio was chosen as $\sigma_s = 2500$ m^{-1}, reflecting the predominance of very small fuel. The two phases (foliage and small branch) considered in the present model have different values of density and surface-to-volume ratio. Based on the experimental measurement of mass fraction, area fraction, and volume fraction of these two phases in the live chaparral shrubs, foliage has $\sigma_s = 3687$ m^{-1} and $\rho_s = 376$ kg/m^3, and branch has $\sigma_s = 1308$ m^{-1} and $\rho_s = 744$ kg/m^3. The moisture content of live chaparral, the water mass fraction based on oven-dry mass of the solid phase, changes with fuel type, season, and environment. In these experiments, the ranges in moisture content of samples burned on the day of collection were 53 to 91% for chamise and 84 to 106% for manzanita. The fuel bed packing ratio ranged from 0.008 to 0.024, and the fuel loading ranged from 2.1 to 8.0 kg/m^2. Ignition of the fuel bed is simulated by introducing a volumetric heat source over the entire fuel bed depth and along a length of 20 cm. This heat supply is maintained until 70% of fuel in the ignition zone is burnt out.

The mass fraction of atmospheric moisture is calculated from the relative humidity. Ambient temperature and relative humidity are known to play important roles in wildfire spread. These environmental effects were considered in the current model.

5. Results and discussion

An extensive experimental study was completed to analyze the important fuel and environmental variables that determine propagation success in laboratory-scale fires in chaparral fuels. Because the response variable (spread success) was binary (yes or no), a stepwise logistic regression method is used to estimate the parameters of a statistical model to predict the probability of fire spread success. The fitted statistical model for predicting the probability (Pr) of successful fire spread was developed as [23]

$$\Pr(\text{spread} = \text{yes}) = e^X/(1 + e^X), \tag{27}$$

where $X = -0.58 + 5.62U + 17\tan\theta + 2.72L + 0.27T_a - 0.25M$. According to the calculated odds ratio, five variables, in decreasing order of importance—wind speed (U, m/s), dry fuel loading (L, kg/m^2), terrain slope percent ($100\tan\theta$, %), fuel moisture content (M, %), and environmental temperature (T_a, °C)—were selected to predict the probability. This

model correctly classified nearly 96% of the 115 experimental fires; however, all possible combinations of experimental and fuel conditions were not equally replicated in the data set.

Based on this experimental result, fire spread in chaparral fuel bed was simulated under different conditions. In the following subsections, a successful fire spread case is first illustrated to reveal the flame structure and to identify the principal mechanisms of heat transfer contributing to the success of fire spread. By comparing numerical results obtained from unsuccessful and successful fire spread cases, the effects of fuel moisture content, fuel bed arrangement, wind, slope, ambient temperature, and humidity on marginal burning state are analyzed.

5.1. A successful fire spread

As a baseline case, we present results for a successful fire spread over a flat fuel bed with no wind. The results show that the propagation of the fire in the fuel bed begins with an initial phase of growth, following which the fire achieves a quasi steady-state. Figs. 4a and 4b show the instantaneous gas-phase temperature contours and velocity vectors 80 and 230 s after initial ignition, respectively. The fuel bed depth is 0.4 m with green fuel loading of 5.5 kg/m^2. The fuel moisture content $M = 60\%$. The corresponding dry fuel loading is $L = 3.4$ kg/m^2. The ambient temperature $T_a = 37\,°C$, and relative humidity $RH = 30\%$; this models the typical summer climate condition in Southern California. Based on these conditions, the fire spread success probability calculated from Eq. (27) is 97%. Fig. 4 shows that the calculated fire spread is successful and that fire propagates from the left to the right end of the fuel bed. The spread rate approximated from temperature contours is 0.23 m/min. Under similar conditions, the fire spread rate observed over the course of several repetitions ranged from 0.13 to 0.22 m/min. The calculated fire spread rate was slightly faster than the experimental value. As mentioned earlier, the physical and chemical processes such as drying, pyrolysis, and char combustion of chaparral shrub fuel occurring in fire were described in very simple form in the model. Because of the lack of accurate data, the kinetic parameters associated with the rates are taken from a model for pine needles. Furthermore, the variation in properties of live chaparral fuels such as surface area-to-volume ratio, density, moisture content, and heat content also reduce the accuracy of the present model. However, for the purpose of studying the marginal burning state, it is still reasonable to analyze the relative effects of different factors by using the present model.

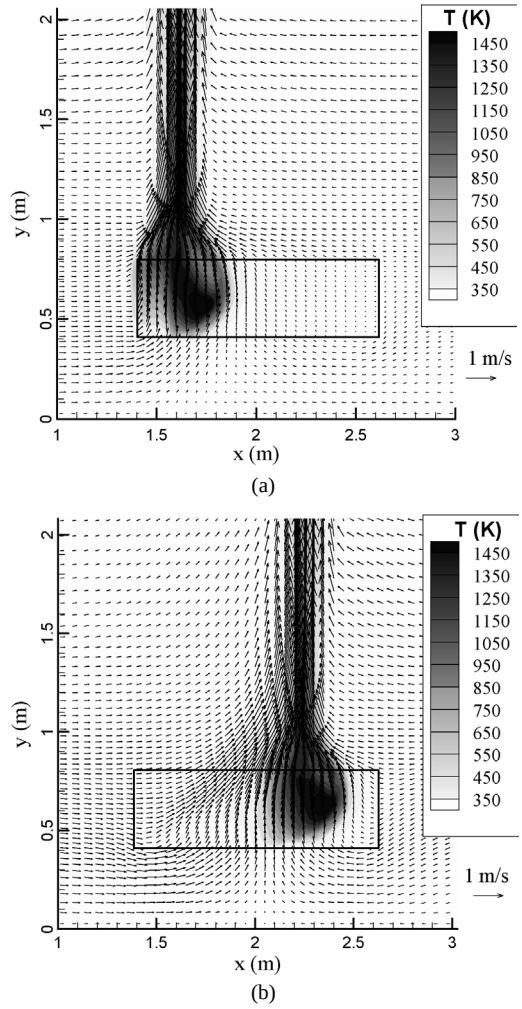

Fig. 4. Time evolution of gas-phase temperature contours and velocity vectors of a successful fire propagation (a) 80 s and (b) 230 s after ignition. The rectangular frame denotes the fuel bed.

As shown in Fig. 4, a plume formed above the burning zone of the fuel bed. The calculated gas-phase temperature field is characterized by two hot zones: in the fuel bed, where heat is released by the homogeneous pyrolysis gas combustion and heterogeneous char combustion, and above the fuel bed, where heat is released only via gas-phase combustion. The velocity field shown in Fig. 4a is characterized by the formation of a hot gas column above the burning zone. The ambient air is entrained into the fire plume. In the thermal plume the gas undergoes an acceleration, the calculated vertical velocity magnitude reaches 1.1 m/s at the top of fuel bed and 4.7 m/s at $y = 2$ m. Within the fuel bed the flow is strongly reduced. Because of the chosen setup of fuel bed, there is a gap between the bottom of the fuel bed and the

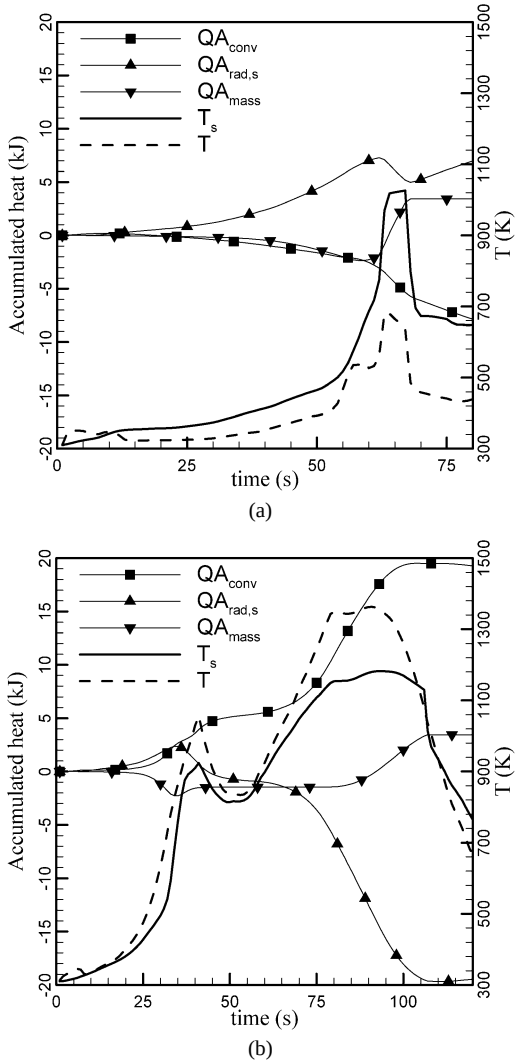

Fig. 5. Time evolution of gas- and solid-phase temperature and accumulated heat absorbed or released by solid particle located 7.5 cm away from the ignition zone and (a) at the bottom of the fuel bed or (b) at the top of the fuel bed.

ground. Thus, fresh air can be entrained from the bottom into the fuel bed. The velocity vectors show an opposed flow induced by the aspired air in the channel between the fuel bed and the ground.

To identify the principal mechanisms of heat transfer contributing to the success of fire spread, we evaluated the accumulated (integrated) value of various heat transfer variables integrated through the burning time as $QA(t) = \int_0^t Q(t')\,\mathrm{d}t'$. Fig. 5 illustrates the time evolution of accumulated heat absorbed (positive value) or released (negative value) by solid particles through three processes: convective heat transfer between gas and solid (Q_{conv}), radiative heat transfer ($Q_{\mathrm{rad,s}}$), and thermochemical contribution (Q_{mass}) due to drying, pyrolysis, and char combustion. These three heat transfer contributions are source terms in the solid-phase heat-conduction equation (Eq. (5)). The time evolution of gas- and solid-phase temperatures is also shown in Fig. 5. To ignite fuel, a solid particle requires sufficient energy to reach its ignition temperature. For a solid particle located at the bottom of the fuel bed and 7.5 cm away from the ignition zone, Fig. 5a reveals the most effective energy source is radiative heat transfer $Q_{\mathrm{rad,s}}$. In the preheat region (0–55 s), solid temperature T_{s} increases slowly with absorbed heat $QA_{\mathrm{rad,s}}$. The thermochemical contribution QA_{mass} remains negative due to water vaporization and pyrolysis. Because the fuel particle is separated from the ignition zone by 7.5 cm, the temperature of the gas phase (T_{g}) is lower than that of the solid phase, leading to a negative value for QA_{conv}. As the flame front moves near the solid particle, the amount of $QA_{\mathrm{rad,s}}$ increases and the moisture is fully released out. Over a short burning time 55–68 s, the solid temperature increases dramatically to 1035 K due to heat release via char combustion. The value of QA_{mass} increases from a negative value to about 3.5 kJ. However, convective heat transfer QA_{conv} still remains negative, which implies a cooling effect of the hot particle. Due to the high value of T_{s}, solid particles start to release heat by radiation which reduces the value of $QA_{\mathrm{rad,s}}$. After 68 s, the solid particle burning is complete and noncombustible ash remains. The value of QA_{mass} stays constant beyond this time.

Because of the cooling effect provided by the aspired air from the bottom of the fuel bed, radiative heat transfer plays a key role in igniting solid fuel and sustaining fire spread. However, at the top surface of the fuel bed, the heat transfer and combustion processes exhibit different roles. Fig. 5b illustrates the time evolution of gas- and solid-phase temperature and accumulated heat transfer QA_{conv}, $QA_{\mathrm{rad,s}}$ and QA_{mass} of a solid particle located at the top of fuel bed and 7.5 cm away with the ignition zone. Because the fire plume is ignited from the bottom of the fuel bed (see Fig. 4), the gas temperature at the top of the fuel bed is higher than solid temperature. The solid particle is preheated by Q_{conv} and $Q_{\mathrm{rad,s}}$, and reaches the burning state at approximately 30 s. At this time, most of the moisture and pyrolysis gases are released and char combustion initiated. It is observed that QA_{mass} starts to increase. When solid temperature reaches $T_{\mathrm{s}} \approx 750$ K, the solid particle loses heat through radiation and hence $QA_{\mathrm{rad,s}}$ decreases. Because the solid particle absorbs heat through Q_{conv} and Q_{mass}, T_{s} increases to about 930 K at 41 s. At this time, the solid particle is noted to be encircled by fire. The oxygen concentration is very low and that leads to termination of char combustion. Over a relatively long period from 41 to 81 s, QA_{mass} stays constant.

The solid temperature decreases to 820 K due to radiative heat loss, and then increases to 1150 K due to convective heating by hot gases. After passage of the fire front, because of aspirated air, char combustion commences again at 81 s and burns out at 107 s. Because of heating through char combustion, both gas and solid temperatures reach their maximum values and then decrease dramatically due to radiative heat loss.

The analysis presented in Fig. 5 denotes the different effects of heat transfer processes on the ignition of solid particles located at the bottom or the top of the fuel bed. In the preheat region, the effect of radiative heat transfer is always positive (heating), but convective heat transfer may be negative (cooling) or positive depending on the gas-phase temperature. The increase in flame height or intensity causes an increase in radiative heat transfer, and also more fresh air is entrained by the fire. These two processes induce, respectively, heating and cooling effects on solid particles located immediately ahead of the flame front.

5.2. Effect of fuel moisture content

The moisture content of wildland fuel has long been recognized as having a major influence on the ignition, development, and spread of fires [45,46]; however, a detailed understanding of the principal mechanisms is lacking. Because higher moisture content implies more heat transfer is needed to dry the fuel, as observed in experiments, it is increasingly difficult for fire to propagate with increasing fuel moisture content. This is also verified by numerical computation, in which the effect of fuel moisture content on ignition of solid particles is included in the term Q_{mass}. Under the same conditions as the baseline case shown in Fig. 4 but with a higher fuel moisture content $M = 70\%$, Fig. 6 illustrates an unsuccessful fire spread case. The distribution of solid fuel mass density and mass fraction isoline (0.3%) of pyrolysis gas (CO) is displayed at two times. At 40 s after initial ignition, Fig. 6a shows a large amount of pyrolysis gas is released, indicating a good burning state. As time evolves to 110 s (Fig. 6b), only a small amount of CO is released, denoting weak burning. Later, fire extinguishes and fire spread terminates. As noted in Fig. 6b, there is an oblique interface along the unburned solid fuel. Because of high moisture content and the cooling effect of fresh air at the bottom of the fuel bed, radiative heating is not sufficient to balance the heat loss due to Q_{mass} and Q_{conv}. The fire starts to extinguish from the bottom and then steadily to the top. This is in conformity with the analysis pertaining to Fig. 5, in which the difference between heat transfer mechanisms at the bottom and the top of the fuel bed was discussed.

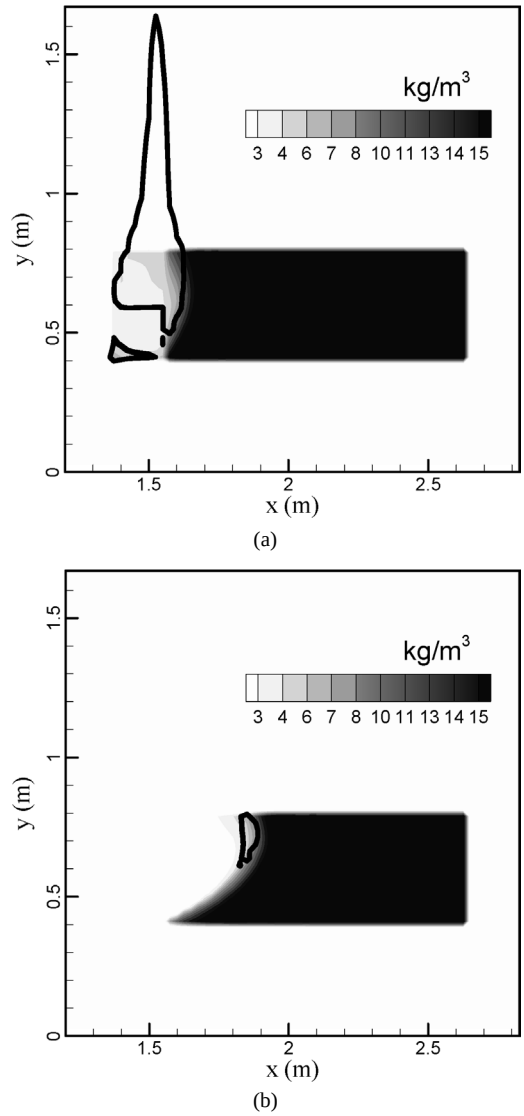

Fig. 6. Time evolution of mass fraction isoline (0.3%) of pyrolysis gas (CO) and distribution of fuel bed mass density (kg/m^3) in the case of unsuccessful fire propagation (a) 40 s and (b) 110 s after ignition.

5.3. Effect of fuel bed arrangement

As seen in Fig. 3, the fuel bed was elevated above the ground to simulate an aerial fuel. If the gap between the fuel bed and the ground is removed and the fuel bed is placed directly on the ground, compared with the unsuccessful case shown in Fig. 6, the numerical computation shows that fire can propagate successfully at the higher moisture content of $M = 70\%$.

Table 1
Effect of the gap between the fuel bed and the ground on fire spread success observed from experiments

Fuel bed arrangement	Fire spread success	Fire spread rate (m/min)
Without gap	Yes	0.139
With gap	No	0.0
Without gap	Yes	0.17
With gap	No	0.0
With gap	No	0.0
Without gap	Yes	0.136

Note. Fuel is ceanothus, RH = 36%, $T_a = 30.6\,^\circ\mathrm{C}$, $L = 2.2\ \mathrm{kg/m^2}$, $\delta = 0.2$ m, $M = 57.4\%$, no wind and slope. For successful fire spread case, the calculated rate is 0.19 m/min. Using Eq. (27) for fire spread case with gap, the calculated probability of fire spread success is 33%.

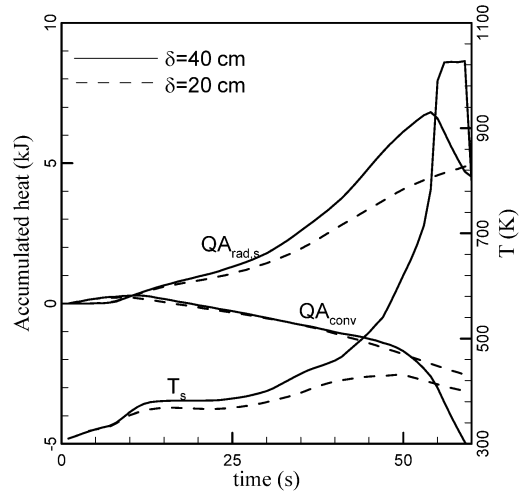

Fig. 7. Effect of fuel bed depth on time evolution of solid particle temperature and accumulated heats absorbed by a solid particle located at the bottom of fuel bed and 5.0 cm away from the ignition zone.

This is mainly because the cooling effect from fresh air acting on the bottom of the fuel bed is reduced with removal of the gap. This numerical result is also supported by our experimental results as shown in Table 1. Under the same experimental conditions and a random running order, Table 1 shows that fire failed to spread when the fuel bed was elevated above the ground, but was successful when the gap was eliminated. For successful spread cases, the observed fire spread rate was 0.14 to 0.17 m/min, compared with the model-predicted rate of 0.19 m/min.

The fuel bed arrangement included variations in fuel loading, fuel bed depth, packing ratio, and fuel particle properties. The experimental work of Burrows [47] revealed that shape, size, composition, and arrangement of fuel particles within a fuel array significantly affect the way in which wildland fires behave. As we discussed the significance of variable σ_s, it was noted that heat transport and absorption by fuel particles, moisture transport into and out of fuels, production rates of volatile combustibles by pyrolysis, diffusion of air, effects of wind, and so forth are all related to fuel surface area. It was expected that, with larger surface area-to-volume ratio, fires would be more likely to burn with higher fuel moisture content. From the experimental observations of extinction and marginal burning studies in woody fuel beds, Wilson [5] developed a predictive rule of thumb based on an extensive experimental data set for fuel beds of dead, woody fuels to determine if fire would burn or not. The rule was that a fire would rarely burn if $M > 0.25\ln(2\sigma_s\beta\delta)$, where β is fuel bed packing ratio, and δ is fuel bed depth. The product $S = \sigma_s\beta\delta$ gives the total fuel surface area per unit horizontal area of fuel bed. This variable was considered in our model (Eq. (27)) by the term L, in which $L = \rho_s\beta\delta$. For live fuel, values of σ_s and ρ_s are usually considered constant. Variables β and δ are related to the fuel bed arrangement. For the same fuel, higher fuel loading means larger packing ratio or greater fuel bed depth.

Compared with the baseline case shown in Fig. 4, the fuel bed depth was reduced to $\delta = 0.2$ m and fuel loading was reduced accordingly to maintain the same β. The numerical result obtained shows that fire spread was terminated after the initial ignition, and the extinction process was similar to the process shown in Figs. 6a and 6b. This result was consistent with experimental observations. Fig. 7 illustrates a comparison of time evolution of solid particle temperature and accumulated heat $QA_{\mathrm{rad,s}}$ and QA_{conv} for two fuel bed depths. Because the locations of solid particles in the two cases were the same, in the preheat region, Fig. 7 shows that QA_{conv} in both cases did not change, but the radiative heat transfer was stronger for $\delta = 0.4$ m than for $\delta = 0.2$ m. This difference in $QA_{\mathrm{rad,s}}$ resulted in a solid temperature $T_s = 1030$ K for $\delta = 0.4$ m, thus causing ignition of the solid fuel. In the case of $\delta = 0.2$ m, T_s increased to 380 K and then decreased to the ambient temperature. Fire was not sustained and fire spread terminated.

Reducing δ or L while keeping β constant meant that the effective fuel surface area S for heat transfer was reduced. This influenced the heat energy absorbed by solid particles. For a successful fire spread case (Fig. 4), Fig. 8 shows the instantaneous distribution of radiative heat intensity absorbed (positive value) or released (negative value) by solid particles in the fuel bed, 80 s after ignition. In the fuel bed, along the flame front, there is a clear interface between negative and positive values. Because the aver-

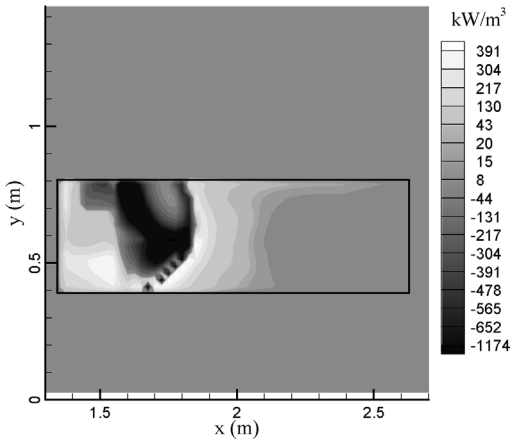

Fig. 8. Internal distribution of radiative heat intensity absorbed (positive value) or released (negative value) by solid particles in the fuel bed denoted by frame. This is a successful fire spread case corresponding to the case shown in Fig. 3.

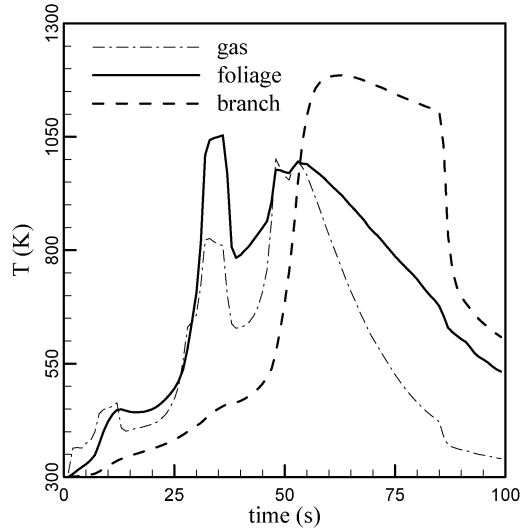

Fig. 9. Time evolution of temperature of gas and solid particles (two phases: foliage and branch) located at the bottom of the fuel bed and 2.5 cm away from the ignition zone.

age optical thickness of the initial fuel bed was about 16 cm ($= 4/\beta\sigma_s$), radiative heat transfer arising from the fire plume over the fuel bed was absorbed mostly by solid particles located at the top surface of the fuel bed. For those particles located at the bottom of the fuel bed, most of the absorbed radiative heat comes from burning embers in the fuel bed. As observed in Fig. 6, the fire extinguished from the bottom of the fuel bed. An increase in fuel bed depth can increase the area of radiative heat transfer through the solid matrix, enabling solid particles to absorb more heat. On the other hand, increased fuel loading means more fuel is consumed and thus the fire intensity is increased. This also increases the amount of heat transfer through radiation. These factors explain why fires would be more likely to burn with higher fuel loading.

In our numerical model the solid fuel is assumed to include two phases, foliage and branch, that have different surface area-to-volume ratios, with $\sigma_s = 3687\ \mathrm{m}^{-1}$ for foliage and $\sigma_s = 1308\ \mathrm{m}^{-1}$ for branches. As evident from Wilson's model [5], a larger value of σ_s promotes solid fuel burning. Fig. 9 illustrates the time evolution of temperature of gas- and solid-phase particles (foliage and branch) located at the bottom of the fuel bed. It is seen that foliage particles are ignited earlier than branch particles. If the fuel bed includes more fine solid fuels, it is easier to achieve a steady fire spread. Observations have indicated that wildfires in chamise usually do not consume material larger than 0.5 in. (1.27 cm) in diameter [45]. To conduct prescribed burning in chaparral, it is important to know the relative amount of fine solid fuel included in fuel bed.

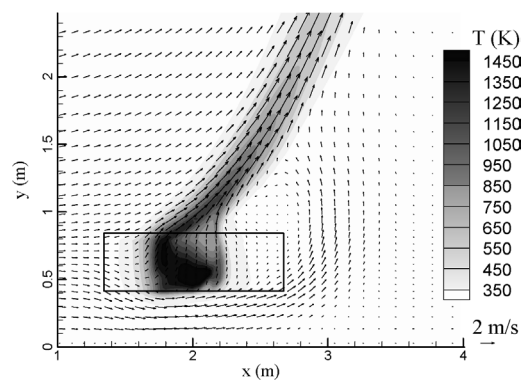

Fig. 10. Wind effect on instantaneous gas-phase temperature and velocity vectors of fire spread in the fuel bed 100 s after ignition.

5.4. Effect of wind

Wind is an important environmental factor that influences wildland fire spread significantly. In southwestern California, dangerous wildfire conditions are created by high-velocity, dry winds known locally as Santa Ana winds. The effect of wind on fire spread has been studied and discussed by many researchers [13,14,16,48]. However, its effect on marginal burning has not received attention. In this article, the effect of wind on marginal burning is discussed briefly. The unsuccessful fire spread case shown in Fig. 6 was calculated again with a wind speed of $U_{\mathrm{ref}} = 1.0$ m/s. Fig. 10 illustrates the instantaneous gas-phase temperature field and velocity vectors at approximately 100 s after ignition. Under the effect of wind, fire

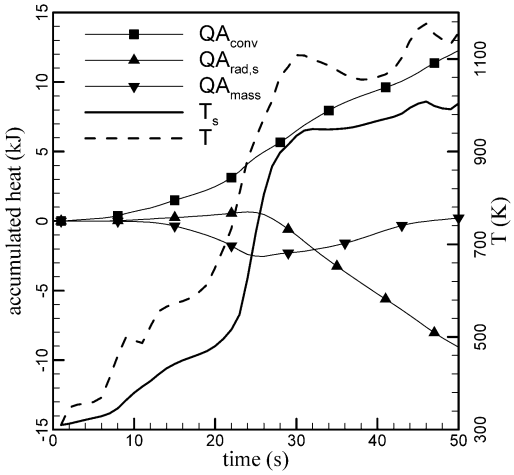

Fig. 11. Wind effect on time evolution of gas- and solid-phase temperature and accumulated heat absorbed by solid particle located at the bottom of the fuel bed and 7.5 cm away from the ignition zone.

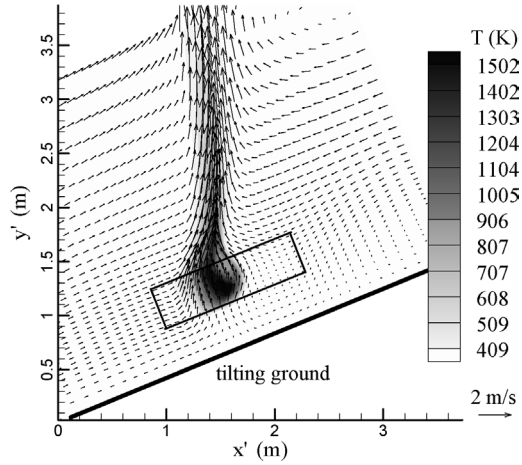

Fig. 12. Slope effect on instantaneous gas-phase temperature field and velocity vectors of fire spread in the fuel bed. There is an angle of 22° between the fuel bed and the horizontal level. The coordinate system (x', y') is rotated an angle from the coordinate (x, y) which is applied in the computation.

spread is successful. This result is supported by experimental data. The effect of the wind blowing from the left side is that the upward movement of flame gases is tilted downward toward the unburnt fuel bed. The shear flow between the hot gas plume and the aspirated fresh air induces vortices. Because of the gap between the bottom of the fuel bed and the ground, fresh air flows with wind into the channel. This vortical movement leads to fresh air being drawn from the right side and also from the bottom of the fuel bed. A detailed examination of Fig. 11 provides insight into how wind helps sustain fire spread at a high fuel moisture content $M = 70\%$. Compared with Fig. 5a, in which the most effective energy source is radiative heat transfer $Q_{\mathrm{rad,s}}$, for the same particle, it is observed that convective heat transfer Q_{conv} plays a more prominent role in igniting a solid particle at approximately 24 s. Although the effect of $Q_{\mathrm{rad,s}}$ is still positive in the preheat region, the hot gas induced by wind takes more energy to heat the solid particle located ahead of the fire front. During the entire burning time shown in Fig. 11, note that the temperature of the gas phase is higher than that of the solid phase. This exchange in heat transfer mechanism induced by wind helps fire to spread successfully at higher fuel moisture content.

5.5. Effect of slope

Topographic slope is one of the essential environmental factors that dramatically influences fire spread. During a prescribed fire, the direction the fire spreads relative to the slope is often used to control fire intensity and fire spread rate [49]. This is because heat transfer, especially radiative heat transfer, is affected by slope. We observed that the marginal burning state was also altered by slope. In this article the effect of slope was simulated by tilting the fuel bed to a slope angle $\theta = 22°$ (slope percent = 40%). The unsuccessful fire spread case shown in Fig. 6 was calculated again (Fig. 12). This is an upslope fire spread case in that the fire was ignited at the lower side and spreads upward. Fig. 12 shows that the upward movement of the fire plume is still vertical but is tilted forward relative to the fuel bed. As analyzed by many researchers [21,22,35–37,50], flames that are tilted forward are closer to the unburned fuel, thereby increasing the radiation heat transfer incident on the fuel, the preheating range, and thus the rate of spread. These factors alter the marginal burning state of chaparral shrub fuel. For high moisture content $M = 70\%$, the computed fire spread is successful, supporting the effect of positive slope in increasing the amount of heat transfer to unburned fuel. This result was also validated by our experimental data.

5.6. Effect of environmental temperature and humidity

In Southern California, the fire season is usually declared in the seasons of summer and fall. This is partly because of high environmental temperature T_{a} and low humidity RH in these seasons. Air temperature is one of several important variables considered when developing a fire "prescription"—the acceptable fuel and environmental conditions under which a fire will be ignited to accomplish specific natural resource management objectives. Air temperature and solar insolation determine fuel temperature. In our ex-

Table 2
Effect of environmental temperature and humidity on fire spread success observed from experiments and calculated from model

Date	T_a (°C)	RH (%)	L (kg/m^2)	Fire spread success	Fire spread rate (m/min)	Calculated rate (m/min)	Calculated probability (%)
8/26/2003	37.3	22	3.32	Yes	0.131	0.22	89.7
8/26/2003	37.3	22	3.32	Yes	0.172	0.22	89.7
11/17/2003	20.2	47	3.24	No	0.0	0.0	14.2
11/17/2003	20.2	47	3.24	No	0.0	0.0	14.2

Note. Fuel is chamise, $\delta = 0.4$ m, no wind and flat fuel bed.

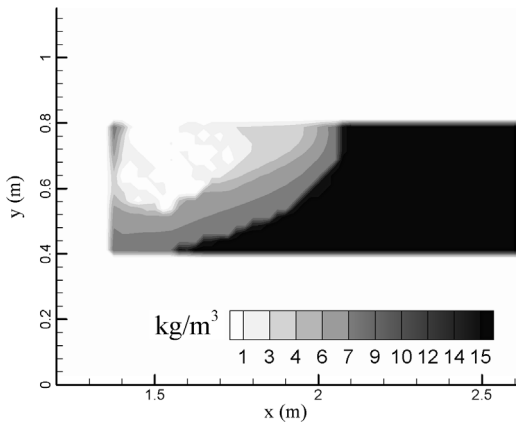

Fig. 13. The final distribution of calculated fuel bed mass density (kg/m^3) of an unsuccessful fire spread at low environmental temperature and high relative humidity.

periments conducted over the course of the calendar year 2003, the values of T_a and RH recorded in different seasons were 18.9 °C and 75% (February 7), 23.9 °C and 43% (May 13), 37.3 °C and 22% (August 26), and 20.2 °C and 47% (November 17). From our experimental results, we observed that the probability of fire spread success would change with T_a and RH. Table 2 illustrates the effect of environmental temperature and humidity on fire spread success. Under similar experimental conditions, fire spread in the "hot" day with calculated probability 89.7% from Eq. (27), but failed on the "cool" day with calculated probability 14.2%. For successful spread cases, the observed fire spread rate was 0.13 to 0.17 m/min but the calculated rate, 0.22 m/min, was a little higher.

Using the same condition as the baseline case shown in Fig. 4 but with a lower $T_a = 20$ °C and higher RH = 70%, the fire spread process from the ignition was calculated again. Fig. 13 illustrates the final distribution of calculated fuel bed mass density. This is an unsuccessful fire spread case in that only a part of solid fuel is consumed after ignition. The extinction process is similar to the process shown in Figs. 6a and 6b. Because of low environmental temperature and high humidity, the cooling effect from the aspirated fresh air is enhanced. Fig. 13 shows an oblique interface along the unburned solid fuel where the fire starts to extinguish from the bottom and then steadily toward the top of the fuel bed. The numerical result is consistent with the experimental observation that a decrease in environmental temperature (or increase of relative humidity) reduces the probability of fire spread success.

6. Conclusion

Motivated by the results of an extensive experimental study, a two-dimensional numerical model was developed to simulate marginal burning state in a live chaparral shrub fuel bed. Such a model was based on a detailed description of the complex interaction between the solid fuel particles and the surrounding gas. The heterogeneous nature of the shrub was taken into account by introducing two phases, viz., foliage and branch. The effects of fuel moisture content, fuel bed arrangement, wind, slope, and environmental temperature and humidity were considered in the numerical model. In modeling the transition between no fire spread and spread under different conditions, numerical results were consistent with the experimental observations. The analysis of numerical results highlighted the effect of various factors on the marginal burning state. It was found that the relative importance of convective and radiative heat transfer processes on the ignition of solid fuel differed with particle location, and could be switched with wind, slope, and fuel bed arrangement. The simulated heat transfer processes and combustion mechanism in the fuel bed are helpful in understanding the overall factors that determine fire spread success.

Direct quantitative comparisons of velocity field, temperature, spread rate, etc., is currently not possible. In the near term, we are seeking more accurate kinetic and thermochemical data for the various chaparral fuels, while continuing to refine various submodels.

Acknowledgments

The funding source for this research is the USDA/USDI National Fire Plan administered through Research Joint Venture Agreement 01-JV-11272166-135

with the Forest Fire Laboratory, Pacific Southwest Research Station, Riverside, CA, USA. S.M. acknowledges partial support from the Wildland Fire R&D Collaboratory, a consortium administered by the National Center for Atmospheric Research.

References

[1] J.S. Fried, C.L. Bolsinger, D. Beardsley, Chaparral in Southern and Central Coastal California in the Mid-1990s: Area, Ownership, Condition, and Change, Resource Bulletin PNW-RB-240, USDA Forest Service, Portland, OR, 2004.
[2] M.C. Carter, C.D. Foster, Forest Ecol. Manage. 191 (2004) 93–109.
[3] L.R. Green, Burning by Prescription in Chaparral, Gen. Tech. Rep. PSW-51, USDA Forest Service, Berkeley, CA, 1981.
[4] A.D. Bruner, D.A. Klebenow, Predicting Success of Prescribed Fires in Pinyon–Juniper Woodland in Nevada, Res. Paper INT-219, USDA Forest Service, Ogden, UT, 1979.
[5] R.A. Wilson Jr., Combust. Sci. Technol. 44 (1985) 179–194.
[6] S. Raybould, T. Roberts, Fire Manage. Note 44 (1983) 7–10.
[7] D. Campbell, The Campbell Prediction System, Wildland Fire Specialists, Ojai, CA, 1995.
[8] W.L. McCaw, Predicting Fire Spread in Western Australian Mallee–Heath Shrubland, Ph.D. dissertation, University of New South Wales, Canberra, 1997.
[9] R.C. Rothermel, A Mathematical Model for Predicting Fire Spread in Wildland Fuels, Res. Paper INT-115, USDA Forest Service, Ogden, UT, 1972.
[10] P.L. Andrews, BEHAVE Fire Behavior Prediction and Fuel Modeling System, Gen. Tech. Rep. INT-194, USDA Forest Service, Ogden, UT, 1986.
[11] J.D. Cohen, Estimating Fire Behavior with Forecast: User's Manual, Gen. Tech. Rep. PSW-90, 1986.
[12] W.H. Frandsen, Combust. Flame 16 (1971) 9–16.
[13] F.E. Fendell, M.F. Wolff, in: E.A. Johnson, K. Miyanishi (Eds.), Forest Fires: Behavior and Ecological Effects, Academic Press, San Diego, 2001.
[14] D. Morvan, J.L. Dupuy, Combust. Flame 138 (2004) 199–210.
[15] A.M. Grishin, in: F. Albini (Ed.), Mathematical Modeling of Forest Fires and New Methods of Fighting Them, Publishing House of Tomsk University, Tomsk, 1992.
[16] B. Porterie, D. Morvan, J.C. Loraud, M. Larini, Phys. Fluids 12 (2000) 1762–1782.
[17] X. Zhou, J.C.F. Pereira, Fire Mater. 24 (2000) 37–43.
[18] D. Morvan, J.L. Dupuy, Combust. Flame 127 (2001) 1981–1994.
[19] D. Morvan, J.L. Dupuy, Combust. Flame 138 (2004) 199–210.
[20] B. Porterie, J.L. Consalvi, A. Kaiss, J.C. Loraud, Numer. Heat Transfer A 47 (2005) 571–591.
[21] P.J. Pagni, T.G. Peterson, Proc. Combust. Inst. 14 (1973) 1099–1107.
[22] F.A. Albini, Combust. Sci. Technol. 45 (1986) 101.
[23] X. Zhou, D. Weise, S. Mahalingam, Proc. Combust. Inst. 30 (2005) 2287–2294.
[24] D. Weise, X. Zhou, L. Sun, S. Mahalingam, Int. J. Wildland Fire 14 (2005) 99–106.
[25] W.L. Fons, H.B. Clements, P.M. George, Proc. Combust. Inst. 9 (1962) 860–866.
[26] C.W. Philpot, Seasonal Changes in Heat Content and Ether Extractive Content of Chamise, Res. Paper INT-61, USDA Forest Service, Intermountain Forest & Range Experiment Station, Ogden, UT, 1969.
[27] R.A. Susott, Forest Sci. 28 (1982) 404–420.
[28] F.P. Incropera, D.P. DeWitt, Fundamentals of Heat and Mass Transfer, fifth ed., Wiley, New York, 2002.
[29] W.P. Jones, B.E. Launder, Int. J. Heat Mass Transfer 15 (1972) 301–314.
[30] R. Clift, J.R. Grace, M.E. Weber, Bubbles, Drops, and Particles, Academic Press, New York, 1978.
[31] U. Svensson, K. Haggkvist, J. Wind Eng. Ind. Aerodyn. 35 (1990) 201–211.
[32] M.H. Kobayashi, J.C.F. Pereira, M.B.B. Siqueira, J. Wind Eng. Ind. Aerodyn. 53 (1994) 357–374.
[33] B.F. Magnussen, B.H. Hjertager, Proc. Combust. Inst. 16 (1976) 719–729.
[34] B.F. Magnussen, B.H. Hjertager, J.G. Olsen, D. Bhaduri, Proc. Combust. Inst. 17 (1978) 1383–1393.
[35] N.J. de Mestre, E.A. Catchpole, D.H. Anderson, R.C. Rothermel, Combust. Sci. Technol. 65 (1989) 231–244.
[36] F. Morandini, P.A. Santoni, J.H. Balbi, Fire Saf. J. 36 (2001) 519–543.
[37] P.J. Pagni, J. Heat Transfer Trans. ASME Ser. C 97 (1975) 153–155.
[38] M.F. Modest, Radiative Heat Transfer, McGraw–Hill, New York, 1993.
[39] B.W. Butler, Experimental measurements of radiant heat fluxes from simulated wildfire flames, in: Proceedings of 12th Conference on Fire and Forest Meteorology, Jekyll Island, GA, October 1993, pp. 104–112.
[40] C. Kaplan, C.R. Shaddix, K.C. Smyth, Combust. Flame 106 (1996) 392–405.
[41] H.A. Anderson, Mechanisms of Fire Spread, Res. Prog. Report No. 1, Res. Paper INT-8, U.S. Forest Service, Intermountain Forest and Range Experiment Station, 1964.
[42] B.M. Wotton, R.S. McAlpine, M.W. Hobbs, Int. J. Wildland Fire 9 (4) (1999) 247–253.
[43] W.R. Catchpole, E.A. Catch, B.W. Butler, R.C. Rothermel, G.A. Morris, D.J. Latham, Combust. Sci. Technol. 131 (1998) 1–37.
[44] S.V. Patankar, Numerical Heat Transfer and Fluid Flow, Hemishpere, New York, 1980.
[45] C.M. Countryman, C.W. Philpot, Physical Characteristics of Chamise as a Wildland Fuel, Res. Paper PSW-66, USDA Forest Service, Berkeley, CA, 1970.
[46] G.M. Jemison, J. Agric. Res. 51 (1935) 885–906.
[47] N.D. Burrows, Int. J. Wildland Fire 10 (2001) 137–143.
[48] W.M. Pitts, Prog. Energy Combust. Sci. 17 (1991) 83–134.
[49] L.R. Green, Burning by Prescription in Chaparral, Gen. Tech. Rep. PSW-51, USDA Forest Service, 1981, pp. 1–36.
[50] D.R. Weise, G.S. Biging, Forest Sci. 43 (1997) 170–180.